DOI: 10.1002/anie.201204478

Visualization of Electrodes

4D Visualization of a Cathode Catalyst Layer in a Polymer Electrolyte Fuel Cell by 3D Laminography–XAFS**

*Takahiro Saida, Oki Sekizawa, Nozomu Ishiguro, Masato Hoshino, Kentaro Uesugi, Tomoya Uruga, Shin-ichi Ohkoshi, Toshihiko Yokoyama, and Mizuki Tada**

Polymer electrolyte fuel cells (PEFCs) are promising sustainable power sources, and Pt and Pt-based alloys are now used as electrocatalysts in practical PEFCs. Although their high energy efficiency enables clean power generation, serious issues regarding cell performance, durability, and cost must be tackled to realize the widespread commercialization of fuel-cell vehicles. A particular problem is the degradation of cathode catalyst by fluctuations in the cathode potential under variable loads and during startup and shutdown.[1]

The details of the cathode catalyst degradation and the factors behind it have not yet been fully investigated because of a lack of characterization methods for directly observing the internal structures and chemical states of the cathode catalyst layer inside membrane electrode assemblies (MEAs). The degradation in the cathode catalyst layer is thought to be caused by various factors,[1] and a number of electrochemical and spectroscopic analyses have been conducted to determine the structures and behaviors of cathode catalysts in MEA of PEFCs. However, it is still difficult to directly provide three-dimensional information on the structure/morphology, distribution, and chemical states of Pt nanoparticle cathode catalysts in MEAs in a non-destructive manner.

The spatial visualization of PEFCs has become a state-of-the-art topic for understanding various phenomena in MEA relevant to the performance and property of PEFC.[2–4] Several studies have examined the visualization of the diffusion of oxygen[2] and water,[3,4] which directly influence fuel-cell performance by regulating the oxygen reduction reaction at the cathode and the proton conductivity in MEAs. Inukai et al. reported the relationship between oxygen partial pressure and the length of gas flow channels by using a dye film.[2] The distribution of water penetration into gas diffusion layers in PEFCs has been observed by X-ray computed tomography (XCT).[4]

XCT is a typical method for obtaining three-dimensional images of a sample, in which the sample is rotated about an axis perpendicular to the incident X-ray beam, and a three-dimensional image is computationally reconstructed.[4–7] XCT has been applied to solid catalysts for syngas conversion by Beale and Weckhuysen and to electrode materials of a lithium–sulfur battery by Nelson et al. to monitor reactive parts and their chemical states.[5–7] Furthermore, XCT can be applied to a sample smaller than observation field area in all projected directions of XCT, but it cannot analyze a flat sample. On the other hand, X-ray computed laminography (XCL) is applicable to partial three-dimensional imaging of a such-shaped sample.[8] In XCL, the rotation axis of a sample is not fixed at 90° with respect to incident X-ray beam, and the sample is inclined (Supporting Information, S1 and Figure S1). Hoshino et al. have developed an XCL system with submicrometer spatial resolution and they obtained three-dimensional images of Cu grids.[9]

Herein, we report the four-dimensional visualization of structures/chemical states of a Pt/C cathode catalyst layer in MEAs of PEFC by a newly developed laminography–X-ray absorption fine structure (XAFS) method combining three-dimensional XCL imaging and XAFS spectroscopy. XAFS has been widely used as a powerful tool to monitor local structures of metal catalysts. Series of XCL images were recorded by changing the energies of incident X-rays, and three-dimensional laminography–XANES (X-ray absorption near-edge structure) spectra of the cathode catalyst layer in the entirety of the MEAs were successfully reconstructed. A similar calculation method for full-field transmission X-ray microscopy (TXM) and XANES spectroscopy to follow 2D- and 3D-morphological and chemical changes of battery electrodes was reported by Meirer et al.[7] The 3D-laminography–XANES method enabled not only imaging of the three-dimensional distribution of Pt nanoparticle catalysts in

[*] Dr. T. Saida, N. Ishiguro, Prof. Dr. T. Yokoyama, Prof. Dr. M. Tada
Institute for Molecular Science
38 Nishigo-naka, Myodaiji, Okazaki, Aichi 444-8585 (Japan)
E-mail: mtada@ims.ac.jp
Dr. O. Sekizawa, Prof. Dr. T. Uruga
Innovation Research Center for Fuel Cells
The University of Electro-Communications
Chofu, Tokyo 182-8585 (Japan)
N. Ishiguro, Prof. Dr. S. Ohkoshi
Department of Chemistry, Graduate School of Science
The University of Tokyo
Hongo, Bunkyo-ku, Tokyo 113-0033 (Japan)
Dr. M. Hoshino, Dr. K. Uesugi, Prof. Dr. T. Uruga
Japan Synchrotron Radiation Research Institute, SPring-8
Koto, Sayo, Hyogo 679-5198 (Japan)
Prof. Dr. T. Yokoyama, Prof. Dr. M. Tada
The Graduate University for Advanced Studies (SOKENDAI)
Myodaiji, Okazaki, Aichi 444-8585 (Japan)

[**] We thank Prof. Y. Iwasawa (Univ. Electro-Commun.) and Prof. M. Takata (RIKEN/Univ. Tokyo) for their helpful discussion. We also thank Dr. S. Nakao and M. Saito (IMS) for SEM and TEM measurements. XAFS measurements were performed with the approval of SPring-8 No. 2011A1537 (BL47XU) and No. 2011B1015 (BL01B1). This work was supported in part by the Polymer Electrolyte Fuel Cell Program from the New Energy and Industrial Technology Development Organization (NEDO) of Japan. XAFS = X-ray absorption fine structure.

Supporting information for this article is available on the WWW under http://dx.doi.org/10.1002/anie.201204478.

cathode catalyst layers but also the visualization of the chemical states of the Pt cathode catalysts in fresh and degraded MEAs in a non-destructive manner.

MEAs were commercially prepared ($5 \times 5\ cm^2$ surface area); 50 wt %-Pt/C was used as the cathode catalyst. A fresh MEA was subjected to 4 cycles of current steps held for 30 s each. A degraded MEA was subjected to 150 cycles of aging and 200 cycles of accelerated degradation testing. The average particle sizes of the Pt cathode catalysts in the fresh and degraded MEAs were 3.5 ± 0.9 nm and 5.4 ± 2.1 nm, respectively (Supporting Information, Figure S2). Each MEA has a layered structure: cathode catalyst layer/polymer electrolyte/anode catalyst layer. The MEAs prepared by aging and load cycling in PEFCs were cut into 10×10 mm pieces and clipped by SiC membranes (thickness: 300 nm) for 3D-laminography–XANES measurements. 3D-laminography–XANES spectra were measured at the BL47XU undulator beamline at SPring-8 (Hyogo, Japan). The rotational axis of the MEA was inclined 30° from the normal toward the downstream direction for the XCL measurements. The rotating stage had a ball-bearing track to suppress wobble during the rotation (details of the XCL method is presented in the Experimental Section, Supporting Information, S1, and Figure S1).

The thickness of the cathode catalyst layer of the fresh MEA was about 140–210 μm as observed in a cross-sectional scanning electron microscopy (SEM) image (Supporting Information, Figure S3). XCL at 11.496 keV before Pt L_{III}-edge provided the three-dimensional morphology images of the cathode catalyst layer in the MEAs. In the fresh MEA, many cracks in a random pattern were observed in the SEM and XCL images, while cracks in the degraded MEA, the cathode catalyst layer of which was about 115–210 μm in thickness, were much more conspicuous. The cross-sectional XCL images in the *X*–*Y* plane at 120, 160, and 200 μm in depth (*Z*) suggested that the cracks were distributed throughout the entire cathode catalyst layer.

3D-laminography–XANES were analyzed to obtain both three-dimensional images of the spatial distribution of the Pt nanoparticle catalysts and their chemical states at the cathode catalyst layers in the MEAs. The spatial distribution of the Pt catalysts was visualized by mapping Pt L_{III}-edge intensity, which corresponds to a difference in the intensity of X-ray absorption at 11.572 keV (isosbestic point of Pt and PtO_2; Supporting Information, S2 and Figure S4) from that at 11.496 keV (before the Pt L_{III}-edge). Independently, Pt L_{III}-edge 3D-laminography–XANES spectra were analyzed for every piece of the cathode catalyst layers in the fresh and degraded MEAs to visualize the chemical states of the Pt catalysts.

For the analysis of the 3D-laminography–XANES data, we first reconstructed 3D images of the distributions of Pt nanoparticles in the cathode catalyst layer in the fresh and degraded MEAs (Figure 1). Bright areas indicate high Pt concentration, and dark areas indicate low Pt concentration. In the fresh MEA, Pt nanoparticle catalysts were almost fully loaded throughout the cathode catalyst layer (Figure 1, A1). Two-dimensional projection of Figure 1, A1 onto the *X*–*Y*, *Y*–*Z*, and *Z*–*X* planes clearly suggested that the Pt distribution was mostly uniform in the fresh MEA (Figure 1, A2).

Note that the distribution of Pt catalysts changed markedly in the three dimensions for the degraded MEA (Figure 1, B). There were several spots, colored red, where aggregation of the Pt catalysts was observed (Figure 1, B1). In addition to the bright spots, large cavities were observed in the cross-sectional 3D-laminography–XANES images in the *X*–*Y* plane presented in Figure 1, B1-CS. Penetration of large cavities through the cathode catalyst layer was observed in the *Z*–*X* plane (Figure 1, B2), indicating a possible degradation of the MEA during voltage step processes operated as the accelerated durability test. The Pt distribution was heterogeneous throughout the entire cathode catalyst layer, which suggests that Pt migration, aggregation, and cracking spread throughout the cathode catalyst layer in the degraded MEA.

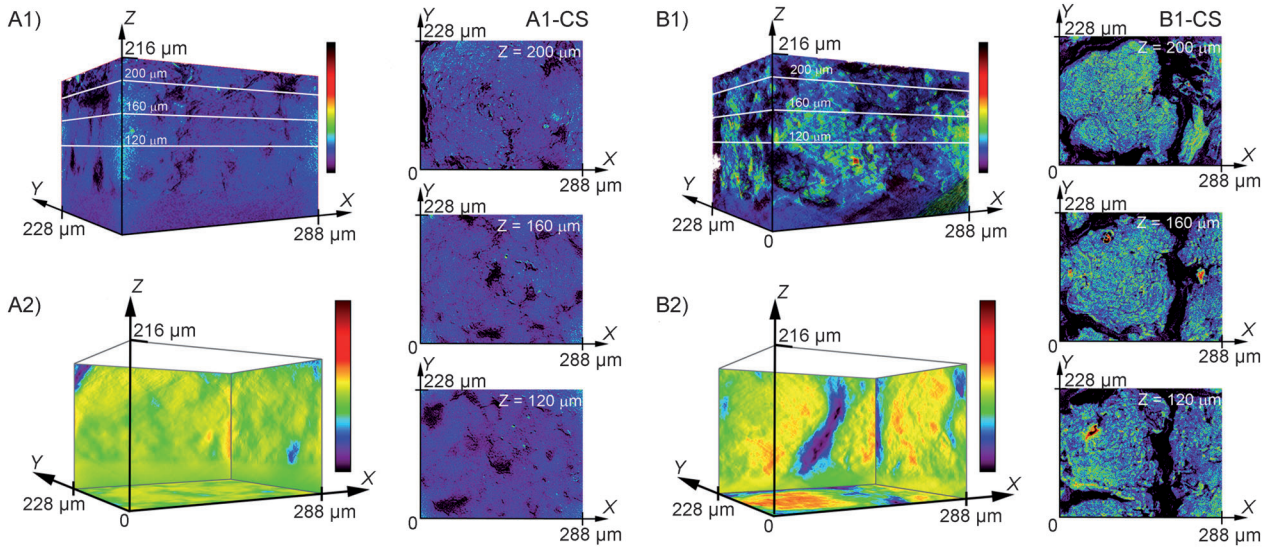

Figure 1. 1) The distribution of Pt catalysts in the cathode catalyst layers of A) fresh and B) degraded MEA as observed by 3D-laminography–XANES. The change in intensity (colored scale bar), which reflects Pt quantity, was calculated from the difference in the intensity of X-ray absorption at 11.572 keV from that at 11.496 keV. CS = Cross-sectional images of (1) in the *X*–*Y* plane at *Z* = 120, 160, and 200 μm. A2), B2) Two-dimensional projections of the summation of the change of intensity onto the *X*–*Y*, *Y*–*Z*, and *Z*–*X* planes of (A1) and (B1).

Depth (Z)-resolved XANES spectra were successfully obtained by integrating 3D-laminography–XANES spectra over the X–Y plane at each depth in the X-ray energy range of 11.439–11.608 keV (Figure 2). A difference in the edge intensity of the Pt L_{III}-edge XANES spectra indicates difference in the Pt quantity in the MEAs along the Z depth. In the fresh MEA, the Pt quantity gradually increased with depth and reached a maximum at about 170 μm deep (Figure 2, A). In contrast, a series of depth-resolved laminography–XANES spectra of the degraded MEA were wavy in the Z direction, which probably reflects the degradation of the MEA (Figure 2, B).

Figure 3 shows 3D-laminography–XANES spectra for particular areas at a depth Z of 113.2 μm; their cross-sectional images of the Pt quantity observed by 3D-laminography–XANES are also presented. In the fresh MEA, no significant aggregation of the Pt catalysts was observed at a depth of 113.2 μm (Figure 3, A). Pt L_{III}-edge 3D-laminography–XANES spectra for two square parts ((a1) and (a2)) were similar to each other, indicating that the Pt catalysts in those areas were in similar chemical states.

In the degraded MEA, the chemical states of the Pt catalysts differed depending on the area/position in the cathode layer. The white-line intensity at the Pt L_{III}-edge of the degraded MEA was higher than that of Pt foil but lower than that in the fresh MEA in the both areas (b1 and b2), as shown in Figure 3, B. In particular, the 3D-laminography–XANES white-line intensity had a lower maximum intensity at the Pt L_{III}-edge in the area where aggregation occurred (b1) than the area where Pt was evenly distributed (b2). The 3D-laminography–XANES spectra indicated the heterogeneous chemical states of the Pt nanoparticle catalysts in the cathode catalyst layer in the degraded MEA, which cannot be monitored by conventional XAFS. It is also suggested that the Pt catalysts in the degraded MEA were in the form of larger Pt nanoparticles with the lower Pt L_{III}-edge white-line intensity.

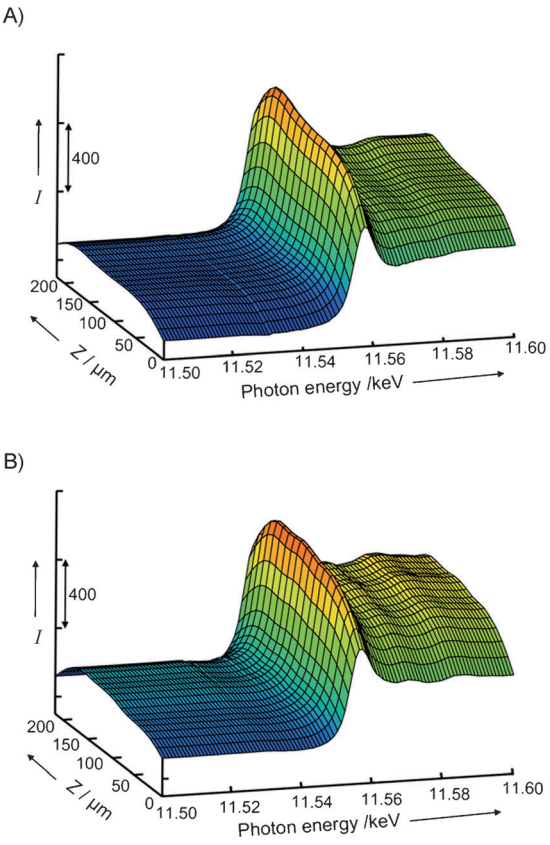

Figure 2. Series of depth-resolved Pt L_{III}-edge laminography–XANES spectra along the Z axis for the cathode catalyst layers in A) fresh and B) degraded MEA. XANES spectra are presented at a depth of every 12 μm.

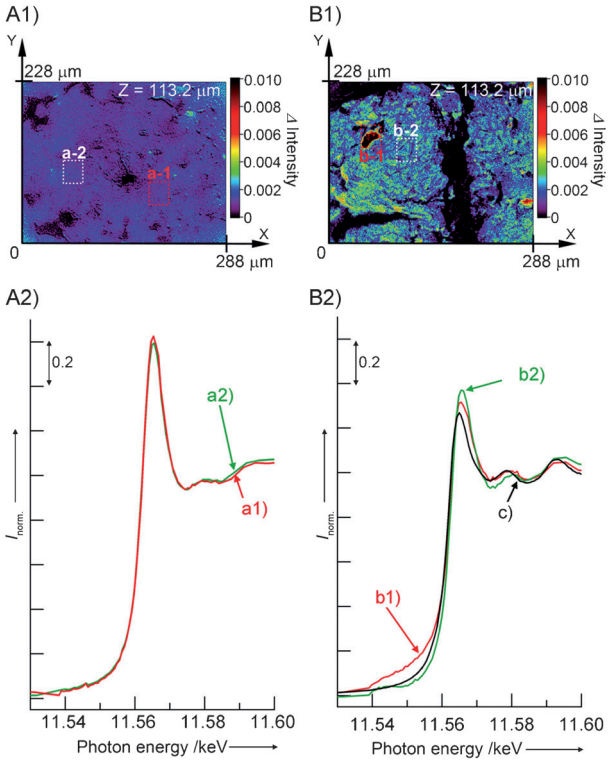

Figure 3. Spatially resolved Pt L_{III}-edge laminography–XANES spectra at a depth Z of 113.2 μm for the catalyst layers in A) fresh and B) degraded MEA. Vertical axis (intensity) was normalized by Pt L_{III}-edge jump. Cross-sectional images represent Pt quantity observed by 3D-Laminography XANES. a1), a2), b1), and b2) ($\Delta X = 27.6$ μm and $\Delta Y = 32.4$ μm) in the cross-sectional images represent measured areas of the corresponding Laminography-XANES spectra. c) XANES spectrum of Pt foil.

Pt L_{III}-edge 3D-laminography–XANES spectra, which reflect the chemical states of the Pt catalysts, were different at every part of the MEA, as shown in Figure 3, whereas conventional XANES method average three-dimensional structural information with different chemical states inside the MEA. Indeed, the 3D-laminography–XANES spectra integrated for the entire cathode catalyst layer agreed with their XANES spectra measured by the conventional XANES (Supporting Information, Figure S5). Pt nanoparticles on carbon supports have been reported to migrate with ease under the durability testing conditions, resulting in dissolution, detachment, and agglomeration.[10] Indeed, we observed large aggregated areas of micrometer size in the XCL images of the degraded MEA. The degradation process of cathode catalyst layer is suggested as follows: the dissolution of Pt catalyst nanoparticles on carbon support and the corrosion of

the carbon support proceed; then the detachment and agglomeration of the Pt nanoparticles are promoted by the collapse of the carbon support; finally, a Pt aggregation area (such as Figure 3, B1) may form in the MEA. In situ laminography–XANES would potentially reveal the degradation mechanism of Pt nanoparticle catalysts at each part of a cathode catalyst layer in a practical PEFC under the operating conditions.

In conclusion, XANES combined with the XCL method (laminography–XANES) has been successfully developed for the four-dimensional visualization of the structure/morphology, Pt distribution, and chemical states of the cathode catalyst layer in MEAs for PEFC in a non-destructive manner. The three-dimensional images of Pt quantity in fresh and degraded MEAs enabled the visualization of aggregation behavior induced under voltage-cycling processes. The spatially-resolved three-dimensional laminography–XANES revealed the heterogeneous presence of aggregation and chemical states of the Pt nanoparticle catalysts in the MEA. The 3D-laminography–XAFS method is promising for visualizing heterogeneous structural information in MEAs to address critical issues on the performance and property of practical PEFCs.

Experimental Section

MEAs were commercially prepared (EIWA Co. Ltd.; $5 \times 5\ cm^2$ surface area); 50 wt% Pt/C (TEC10E50E; Tanaka Kikinzoku Kogyo Co. Ltd. (TKK)) was used as cathode catalyst with Pt loading of $6.0\ mg\,cm^{-2}$, and 50 wt%-Pd/C (TECPd(ONLY)E50E; TKK) was used as anode catalyst with Pd loading of $0.5\ mg\,cm^{-2}$. A fresh MEA was subjected to four cycles of current steps held for 30 s each. A degraded MEA was subjected to 150 cycles of aging and 200 cycles of accelerated degradation testing. Averaged particle sizes of the Pt catalysts were estimated by TEM (Supporting Information, Figure S2).

A high spatial resolution X-ray image detector was used, which was consisted of a visible-light conversion unit, called a beam monitor (BM3, AA50, Hamamatsu Photonics, K. K.), and a cooled charge-coupled device (CCD) camera (C-4880–41S, 4000 (H) × 2624 (V) pixels, 5.9 μm/pixel, Hamamatsu Photonics, K.K.). Incident X-ray beam to the detector was converted into visible light by a LSO (Lu_2SiO_5:Ce) crystalline scintillator, and the visible-light image was focused onto the CCD camera using a microscope objective (approximately 50×). As the CCD camera was used as 4 × 4 binning mode, the effective pixel size and field of view of the transmission image were 0.4 μm/pixel and 400 (H) × 262 (V) μm, respectively. Consequently, a field of view of the sectional image (*X*–*Y* section) obtained from laminography reconstruction was then $400 \times 400\ \mu m^2$.

Transmission images of MEA samples were acquired by 360° rotation to obtain three-dimensional data. The number of transmission images was 1800 per energy scan. Sectional images were reconstructed using a filtered back-projection method by considering the inclination of the rotational axis. A three-dimensional image was constructed by stacking *X*–*Y* sectional images along the *Z* axis. In the laminography reconstruction, however, it is impossible to reconstruct a complete three-dimensional image because of the inclination of the rotational axis. Therefore, there is a difference of spatial resolution depending on the direction of the reconstructed three-dimensional image: the actual spatial resolution in the reconstructed *X*–*Y* plane was 1.5 μm, while the spatial resolution in the depth (*Z*) direction was about 5 μm.

83 XCL images were measured for 3D-laminography–XANES in the photon energy range of 11.394–11.609 keV. Energy intervals were 16.6 eV (11.394–11.538 keV), 0.7 eV (11.539–11.584 keV), and 3.5 eV (11.588–11.609 keV). The 3D-laminography–XANES measurements were performed for about 28 h/sample (20 min/energy).

Received: June 9, 2012
Published online: September 11, 2012

Keywords: catalyst degradation · fuel cells · imaging · laminography · XANES

[1] a) R. Borup, J. Meyers, B. Pivovar, Y. S. Kim, R. Mukundan, N. Garland, D. Myers, M. Wilson, F. Garzon, D. Wood, P. Zelenay, K. More, K. Stroh, T. Zawodzinski, J. Boncella, J. E. McGrath, M. Inaba, K. Miyatake, M. Hori, K. Ota, Z. Ogumi, S. Miyata, A. Nishikata, Z. Siroma, Y. Uchimoto, K. Yasuda, K. Kimijima, N. Iwashita, *Chem. Rev.* **2007**, *107*, 3904; b) F. A. de Bruijn, V. A. T. Dam, G. J. M. Janssen, *Fuel Cells* **2008**, *8*, 3; c) X. Yu, S. Ye, *J. Power Sources* **2007**, *172*, 145.

[2] J. Inukai, K. Miyatake, K. Takada, M. Watanabe, T. Hyakutake, H. Nishide, Y. Nagumo, M. Watanabe, M. Aoki, H. Takano, *Angew. Chem.* **2008**, *120*, 2834; *Angew. Chem. Int. Ed.* **2008**, *47*, 2792.

[3] a) H. Iwase, S. Koizumi, H. Iikura, M. Matsubayashi, D. Yamaguchi, Y. Maekawa, T. Hashimoto, *Nucl. Instrum. Methods Phys. Res.* **2009**, *605*, 95; b) S. J. Lee, N.-Y. Lim, S. Kim, G.-G. Park, C. -So Kim, *J. Power Sources* **2008**, *185*, 867; c) Z. Wu, C.-S. Wu, P. P.-J. Chu, S. Ding, *Magn. Reson. Imaging* **2009**, *27*, 871.

[4] a) P. K. Sinha, P. P. Mukherjee, C.-Y. Wang, *J. Mater. Chem.* **2007**, *17*, 3089; b) T. Mukaide, S. Mogi, J. Yamamoto, A. Morita, S. Koji, K. Takada, K. Uesugi, K. Kajiwara, T. Noma, *J. Synchrotron Radiat.* **2008**, *15*, 329; c) S.-J. Lee, S.-G. Kim, G.-G. Park, C.-S. Kim, *Int. J. Hydrogen Energy* **2010**, *35*, 1054; d) I. Manke, C. Hartnig, N. Kardjilov, H. Riesemeier, J. Goebbels, R. Kuhn, P. Krüger, J. Banhart, *Fuel Cells* **2010**, *10*, 26; e) T. Sasabe, P. Deevanhxay, S. Tsushima, S. Hirai, *Electrochem. Commun.* **2011**, *13*, 638; f) R. Flückiger, F. Marone, M. Stampanoni, A. Wokaun, F. N. Büchi, *Electrochim. Acta* **2011**, *56*, 2254.

[5] a) A. Sakdinawat, D. Attwood, *Nat. Photonics* **2010**, *4*, 840; b) J.-D. Grunwaldt, C. G. Schoer, *Chem. Soc. Rev.* **2010**, *39*, 4741.

[6] a) A. M. Beale, S. D. M. Jacques, J. A. Bergwerff, P. Barnes, B. M. Weckhuysen, *Angew. Chem.* **2007**, *119*, 8988; *Angew. Chem. Int. Ed.* **2007**, *46*, 8832; b) M. G. O'Brien, S. D. M. Jacques, M. D. Michiel, P. Barnes, B. M. Weckhuysen, A. M. Beale, *Chem. Sci.* **2012**, *3*, 509; c) M. W. Zandbergen, S. D. M. Jacques, B. M. Weckhuysen, A. M. Beale, *Angew. Chem.* **2012**, *124*, 981; *Angew. Chem. Int. Ed.* **2012**, *51*, 957.

[7] a) F. Meirer, J. Cabana, Y. Liu, A. Mehta, J. C. Andrews, P. Pianetta, *J. Synchrotron Radiat.* **2011**, *18*, 773; b) J. Nelson, S. Misra, Y. Yang, A. Jackson, Y. Liu, H. Wang, H. Dai, J. C. Andrews, Y. Cui, M. F. Toney, *J. Am. Chem. Soc.* **2012**, *134*, 6337.

[8] a) L. Helfen, T. Baumbach, P. Mikulík, D. Kiel, P. Pernot, P. Cloetens, J. Baruchel, *Appl. Phys. Lett.* **2005**, *86*, 071915; b) S. Harasse, W. Yashiro, A. Momose, *Opt. Express* **2011**, *19*, 16560; c) L. Helfen, A. Myagotin, P. Mikulík, P. Pernot, A. Voropaev, M. Elyyan, M. D. Michiel, J. Baruchel, T. Baumbach, *Rev. Sci. Instrum.* **2011**, *82*, 063702.

[9] M. Hoshino, K. Uesugi, A. Takeuchi, Y. Suzuki, N. Yagi, *AIP Conf. Proc.* **2011**, *1365*, 250.

[10] a) K. J. J. Mayrhofer, S. J. Ashton, J. C. Meier, G. K. H. Wiberg, M. Hanzlik, M. Arenz, *J. Power Sources* **2008**, *185*, 734; b) F. J. Perez-Alonso, C. F. Elkjær, S. S. Shima, B. L. Abrams, I. E. L. Stephens, I. Chorkendorff, *J. Power Sources* **2011**, *196*, 6085.

